



# Impact of Emulsifier Structure and Concentration on Lipolysis Dynamics and Curcumin Bioaccessibility in the Nanoemulsions Stabilized by Polyglycerol Fatty Acid Esters

Shangwei Zhang<sup>1</sup> · Xiaofei Xu<sup>2</sup> · Jiguo Yang<sup>1,2</sup> · Jie Ren<sup>2</sup>

Received: 13 February 2021 / Accepted: 18 June 2021

© The Author(s), under exclusive licence to Springer Science+Business Media, LLC, part of Springer Nature 2022

## Abstract

Polyglycerol fatty acid esters (PGFEs), a type of nonionic surfactants, have been widely used in food industry. However, the effects of the aliphatic chain lengths in PGFEs and the concentrations of PGFEs on digestive profiles in emulsion-based systems are poorly understood. The present study has investigated the physicochemical stability, lipolysis dynamics and curcumin bioaccessibility in the nanoemulsions stabilized by synthesized PGFEs with different aliphatic chains (C<sub>10</sub>-C<sub>18</sub>) at various concentrations using an in vitro gastrointestinal tract (GIT) model. Shorter aliphatic chain or higher concentrations of PGFEs resulted in smaller droplets in the emulsions before and during digestion. PGFEs concentration had different impacts on lipolysis dynamics of nanoemulsions depending on the aliphatic chain lengths of PGFEs. Furthermore, long aliphatic chain of PGFEs contributed to a greater rate and extent of lipolysis, but a lower bioaccessibility of curcumin compared with medium ones, which was attributed to the formation of insoluble calcium soaps induced by calcium ions. These results are expected to facilitate the application of PGFEs for developing optimized nanoemulsions in encapsulating poorly water-soluble nutraceuticals in functional food industry.

**Keywords** Polyglycerol fatty acid esters · Nanoemulsions · In vitro digestion · Lipolysis dynamics · Curcumin bioaccessibility

## Introduction

The ongoing COVID-19 pandemic has imposed numerous global challenges. Promoting a healthy living via consumption of functional food to minimize the health impact of SARS-CoV-2 infection and enhance the immune system is a promising strategy [1]. With the increasing needs for functional food characterized by high stability and high absorption attributes, there has been a growing interest in designing emulsion-based delivery systems to encapsulate, protect and deliver lipophilic nutraceuticals, such as oil-soluble vitamins, carotenoids, curcumin and omega-3 fatty

acids in functional food [2]. Typically, nanoemulsion is one of commonly used delivery systems in food formulations due to its simple fabrication and high physical stability [3]. Nanoemulsion is known as a solution system composed of two immiscible liquids, typically lipid phase and aqueous phase, with particle sizes below 200 nm [4]. Owing to their relatively small droplet sizes, nanoemulsions have reported to facilitate lipid digestion and enhance the bioaccessibility of encapsulated nutraceuticals [5]. Therefore, more information on the factors affecting the gastrointestinal (GI) fate of ingested nanoemulsions is required.

It is widely acknowledged that the GI behavior of nutraceutical-loaded emulsions is highly influenced by interfacial composition dependent on original emulsifiers and lipolysis products accumulating at the interfaces [6]. Generally, interfacial composition determines aggregation state of the droplets within the GIT which affects the accessibility of lipase onto the droplet surfaces and therefore lipid hydrolysis [7]. Moreover, interfacial composition also directly impacts the displacement and adsorption of lipase and bile salts at the interfaces, thereby modulating lipid digestion [8]. In

✉ Jiguo Yang  
yangjg@scut.edu.cn

<sup>1</sup> School of Food Science and Engineering, South China University of Technology, 381 Wushan Road, Guangzhou 510641, China

<sup>2</sup> Innovation Center of Bioactive Molecule Development and Application, South China Institute of Collaborative Innovation, Dongguan 221116, China

particular, recent investigations have demonstrated that the chain lengths of oil composition in nanoparticles greatly influence lipolysis profile and nutraceutical bioaccessibility due to the difference in water dispersibility and solubilization capacity of their free fatty acids (FFAs) released [9, 10]. Thus, it can be deduced that the aliphatic chain lengths of lipid-based surfactants may also play an important role on lipid digestion and the micellization of nutraceuticals in the emulsion-based systems.

Polyglycerol fatty acid esters (PGFEs), containing a hydrophilic polyglycerol head group and one or more esterified aliphatic chain tails, have extensive applications in food industry due to their excellent emulsifying capabilities and antimicrobial properties [11, 12]. Functional performance of PGFEs can be varied through the alteration of polymerization degree in glycerol and the aliphatic chain composition. Interestingly, a higher polymerization degree of glycerol in PGFEs resulted in smaller particle sizes and better stability in the nanoemulsions after exposure to gastric fluid [13, 14]. However, little information is available concerning the impact of the aliphatic chain lengths in PGFEs on the GI fate of nutraceutical-enriched emulsions to date. Curcumin exerts a wide range of health-promoting effects, such as anti-inflammatory, antioxidant, anticancer and antimicrobial, which has been shown to be effective against multiple chronic diseases including cancer, diabetes, cardiovascular, neurological, and autoimmune diseases [15, 16]. Due to its poor water solubility and low oral bioavailability, curcumin was selected for encapsulation in PGFEs-stabilized nanoemulsions. The present study investigated the effect of five kinds of PGFEs with different aliphatic chains ( $C_{10}$ - $C_{18}$ ) at various concentrations (unsaturated concentration, saturated concentration and supersaturated concentration) on physicochemical stability, lipolysis dynamics and curcumin bioaccessibility in curcumin-loaded nanoemulsions using an *in vitro* digestion model, to better understanding how the aliphatic chain lengths and the concentrations of PGFEs influence lipolysis dynamics and the bioaccessibility of lipophilic nutraceuticals within the GIT.

## Materials and Methods

### Materials

Glycerol was purchased from Tianjin Damao Chemical Reagent Co., Ltd. (Tianjin, China). Capric acid, lauric acid, myristic acid, palmitic acid and stearic acid were provided by Shanghai Aladdin Biochemical Technology Co., Ltd. (Shanghai, China). Novozym 435 (10,000 PLU/g) was obtained from Novozymes (China) Biotechnology Co., Ltd. (Tianjin, China). Medium chain triglyceride (MCT, 55.50% caprylic triglyceride and 44.50% capric triglyceride) and

curcumin (98%) was acquired from Xi'an Rozen Biotechnology Co., Ltd. (Xi'an, China). Pepsin from porcine gastric mucosa (1:3000, S10030), lipase from porcine pancreas ( $\geq 30,000$  U/g, S10035), and porcine bile salts (S30895) were purchased from Shanghai yuanye Bio-Technology Co., Ltd. (Shanghai, China). All other chemicals and reagents used in the study were of analytical grade. All solutions and nanoemulsions were prepared using deionized water.

### Enzymatic Synthesis of PGFEs

The synthesis and purification of polyglycerols were done according to previously described method [17]. Purified polyglycerols contained diglycerol, triglycerol, tetraglycerol and minor pentaglycerol, with average polymerization degree ( $n$ ) being approximately 2.82 (Fig. S1 and Table S1). Hereafter, purified polyglycerols and designated fatty acids were mixed at a molar ratio of 1:1 (fatty acids/polyglycerols) and reacted with Novozym 435 (2.0%, w/w based on the total substrate mass) for 10 h at 75 °C to acquire corresponding PGFEs. Five kinds of PGFEs were synthesized using fatty acids with different chain lengths ( $C_{10}$ - $C_{18}$ ), including polyglycerol capric acid esters (PGC), polyglycerol lauric acid esters (PGL), polyglycerol myristic acid esters (PGM), polyglycerol palmitic acid esters (PGP) and polyglycerol stearic acid esters (PGS), respectively. Characterized by HPLC-ELSD and ESI-MS as previously reported [17], synthesized PGFEs were mainly composed of monoesters and diesters, while there were minor tristers present in PGFEs with medium aliphatic chain (Fig. S2, Table S2 and S3).

### Preparation of Curcumin-Enriched Nanoemulsions

Curcumin-loaded nanoemulsions were prepared according to a previous methodology with some modifications [18]. Initially, curcumin-enriched oil phase was produced by dispersing curcumin powder (0.2%, w/w) into the MCT and subsequently stirring at 60 °C for 2 h. An emulsifier solution was prepared by dispersing an appropriate amount of PGFEs in phosphate buffer solution (10 mM, pH 6.5) with stirring at 60 °C until completely dissolution. The curcumin-loaded oil phase (5.0%, w/w) and emulsifier solution (95%, w/w) were mixed using a high-shear blender (Ultra Turrax T18, IKA, Staufen, Germany) at 10000 rpm for 2 min, before further processing by a high-pressure homogenizer (JNBIO JN-02C, Guangzhou Juneng Nano&Bio Technology Co., Ltd., Guangzhou, China) at 110 MPa for 5 cycles. The formulated nanoemulsions were used within 3 days and stability was ensured during this period (Fig. S3 and Table S4).

Due to varied emulsifying capabilities among PGFEs, a preliminary experiment was performed to explore PGFEs saturation concentration where nanoemulsions reached fairly constant particle sizes based on a previous study [19].

Fifteen types of nanoemulsions were prepared using five kinds of synthesized PGFEs (PGC, PGL, PGM, PGP and PGS) at three concentrations (unsaturated concentration, saturated concentration and supersaturated concentration), respectively. Specifically, the unsaturated concentration and supersaturated concentration were defined separately as half and twice of the saturated concentration (Table 1). Additionally, nanoemulsions stabilized by PGFEs, PGFEs with medium aliphatic chain, PGFEs with long aliphatic chain, PGC, PGL, PGM, PGP, PGS were abbreviated as PGFE-NEs, medium-chain PGFE-NEs, long-chain PGFE-NEs, PGC-NE, PGL-NE, PGM-NE, PGP-NE and PGS-NE, respectively.

### Particle Characterization

Particle sizes and particle size distributions in the nanoemulsions before and after exposure to simulated gastric and small intestinal phases were determined by static light scattering (Mastersizer 2000, Malvern Instruments, Worcester-shire, UK). Particle sizes were reported as the volume mean diameter.

Electrical charges on the particles before and during in vitro digestion were measured using a particle electrophoresis instrument (Nano ZS, Malvern Instruments, Worcester-shire, UK). The refractive indices of the dispersed phase and the continuous phase were 1.45 and 1.33, respectively. Electrical charges on the droplets were expressed as  $\zeta$ -potential.

### Determination of Curcumin Concentration

Curcumin concentration in the tested samples was measured by a method with some modifications [20]. In brief, an aliquot of sample was diluted to an appropriate concentration with ethanol followed by centrifugation at 10000 rpm for 10 min. Afterwards, the absorbance of supernatant was immediately determined at 425 nm using ethanol as blank. For quantification of curcumin, a standard curve was constructed ( $y = 0.0761x - 0.0084$ ,  $R^2 = 0.9992$ ) (Fig. S4).

**Table 1** Concentrations of PGFEs in nanoemulsions

PGFEs	Aliphatic chain lengths of PGFEs	Concentration (% w/w based on the aqueous mass)		
		Unsaturat-ion	Saturat-ion	Super-saturat-ion
PGC	C <sub>10</sub>	2.0	4.0	8.0
PGL	C <sub>12</sub>	1.0	2.0	4.0
PGM	C <sub>14</sub>	0.5	1.0	2.0
PGP	C <sub>16</sub>	0.25	0.5	1.0
PGS	C <sub>18</sub>	0.25	0.5	1.0

Encapsulation efficiency (EE%) and retention rate of curcumin in nanoemulsions were calculated using the following equations:

$$EE(\%) = \frac{C_{initial}}{C_{oil}} \times 100$$

$$\text{Curcumin retention rate}(\%) = \frac{C_{digesta}}{C_{initial}} \times 100$$

where  $C_{initial}$ ,  $C_{oil}$  and  $C_{digesta}$  are the concentrations of curcumin in the initial nanoemulsions, the oil phase and the digesta at the end of the intestinal digestion ( $\mu\text{g/mL}$ ), respectively.

### In Vitro Digestion

Nanoemulsions were passed through a static simulated GIT model consisting of the stomach and the small intestinal phases to monitor their GI fate [21, 22]. It should be noted that the oral phase was not included, since the studied samples were liquid less affected by the oral digestion.

**Stomach phase:** 20 mL of simulated gastric fluid containing 6.4 mg/mL pepsin was mixed with 20 mL of nanoemulsion. The mixture was then adjusted to pH 3.0 using HCl and incubated for 1 h at 37 °C shaking at 100 rpm.

**Intestinal phase:** 3.5 mL of bile salts solution (53.57 mg/mL), and 1.5 mL of simulated intestinal fluid (7.5 M NaCl and 0.5 M CaCl<sub>2</sub>) were added into 30 mL of the chyme, and the mixture was adjusted to pH 7.0. Hereafter, 2.5 mL of freshly prepared lipase suspension (24 mg/mL) was immediately added to initiate lipolysis reaction. The final concentration of bile salts, CaCl<sub>2</sub> and lipase in the mixture was 5 mg/mL, 20 mM and 1.6 mg/mL, respectively. Lipolysis profile was monitored by titrating 0.25 M NaOH solution into the mixture to maintain a constant pH value ( $\text{pH } 7.00 \pm 0.02$ ) over 2 h. Lipolysis profile was expressed as released FFAs (%) during the small intestinal phase calculated by the following formula:

$$FFAs(\%) = 100 \times \left( \frac{V_{NaOH} \times C_{NaOH} \times M_{oil}}{W_{oil} \times 2} \right)$$

where  $V_{NaOH}$  is the volume (L) of NaOH solution consumed to neutralize the FFAs released during digestion,  $C_{NaOH}$  is the molarity of NaOH solution used (mol/L),  $M_{oil}$  is the molecular weight of MCT (considered to be 521 g/mol), and  $W_{oil}$  is the weight of MCT submitted into lipolysis (g). Blanks (PGFEs solutions without oil) were also run, and the volume of NaOH consumed for blanks was subtracted from that used for the corresponding PGFE-NEs, to get the lipolysis of lipid droplets in the emulsions without the influence of PGFEs hydrolysis. Additionally, bulk oil (curcumin dissolved in MCT) was used as control.

At the end of lipolysis, the digesta was centrifuged (Sigma 3 K15, Sigma Laborzentrifugen GmbH, Osterode

am Harz, Germany) at 12000 rpm for 30 min at 4 °C, and the clear supernatant obtained was collected and considered as the micellar fraction. Micellar transfer rate of curcumin (MT%) and curcumin bioaccessibility (BC%) were calculated by the following equations:

$$MT(\%) = \frac{C_{micelle}}{C_{digesta}} \times 100$$

$$BC(\%) = \frac{C_{micelle}}{C_{initial}} \times 100$$

where  $C_{initial}$ ,  $C_{digesta}$  and  $C_{micelle}$  are the concentrations of curcumin in the initial nanoemulsions, the digesta at the end of the intestinal digestion, as well as the micelles ( $\mu\text{g/mL}$ ), respectively.

### Modeling of Lipolysis Dynamics

A three-parameter logistic model has been developed to elucidate the amount of FFAs released as a function of digestion time [23]. In the present study, released FFAs (%) during lipolysis was fitted to the following formula using a nonlinear analysis in Origin 9.0 software (Origin Lab, Northampton, Massachusetts, USA):

$$C(t) = \frac{C_f}{1 + e^{k(T_c - t)}}$$

where  $C(t)$  is released FFAs (%) when digestion time is  $t$ ,  $C_f$  is the asymptotic value when digestion time is  $\infty$ ,  $k$  is the rate constant ( $\text{min}^{-1}$ ),  $T_c$  is the time to achieve effective lipolysis where half the FFAs are released (min). Additionally, adjusted  $R^2$  of all estimated curves in this work were greater than 0.98, suggesting the great fitness of this model for lipolysis profiles (data not shown).

### Statistical Analysis

All experiments were performed in triplicate and the results were expressed as mean  $\pm$  standard deviation (SD). Statistical analysis was done by one-way analysis of variance (ANOVA) and Tukey multiple-comparison test using Origin 9.0 software.  $p < 0.05$  was considered as statistically significant.

## Results and Discussion

### Physicochemical Stability within the GIT

Physicochemical stability of PGFE-NEs during in vitro digestion were determined in terms of particle sizes, particle size distributions and  $\zeta$ -potential and curcumin level.

### Particle Sizes and Particle Size Distributions

All the initial PGFE-NEs contained small particle sizes (below 200 nm) presenting monomodal particle distributions (Figs. 1a and 2a), suggesting all PGFEs were capable of producing stable nanoemulsions. Further, particle sizes of PGFE-NEs decreased with an increase in PGFEs concentrations until they reached constant sizes over the saturated concentration. Based on the preliminary experiment, the saturated concentrations of PGFEs were independently 4.0, 2.0, 1.0, 0.5 and 0.5% (w/w) for PGC, PGL, PGM, PGP and PGS, and particle sizes in corresponding nanoemulsions were  $97.3 \pm 1.0$ ,  $111.7 \pm 0.4$ ,  $125.4 \pm 0.4$ ,  $141.0 \pm 0.6$ ,  $154.0 \pm 0.9$  nm, respectively (Table S5). Longer aliphatic chain of PGFEs were more effective at saturating droplet

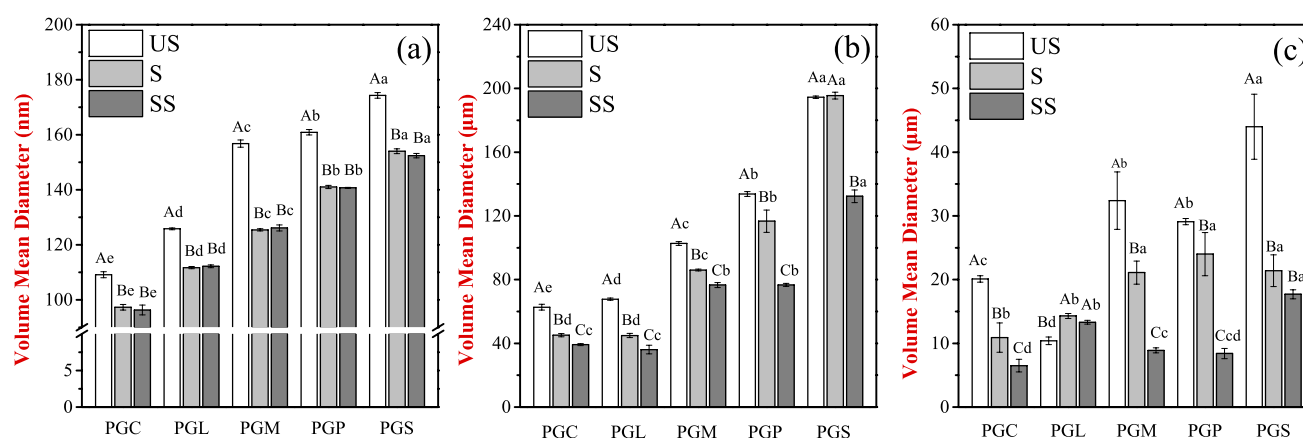


**Fig. 1** Volume mean diameter of nanoemulsions stabilized by PGFEs at different concentrations. **a** initial phase; **b** stomach phase; **c** intestinal phase. Different capital letters indicate significant differences ( $p < 0.05$ ) among nanoemulsions stabilized by the same PGFEs at different concentrations. Different lowercase letters indicate significant

differences among nanoemulsions stabilized by different PGFEs at concentrations of the same saturation degree (the same gray scale in bars). US = at the unsaturated concentration; S = at the saturated concentration; SS = at the supersaturated concentration

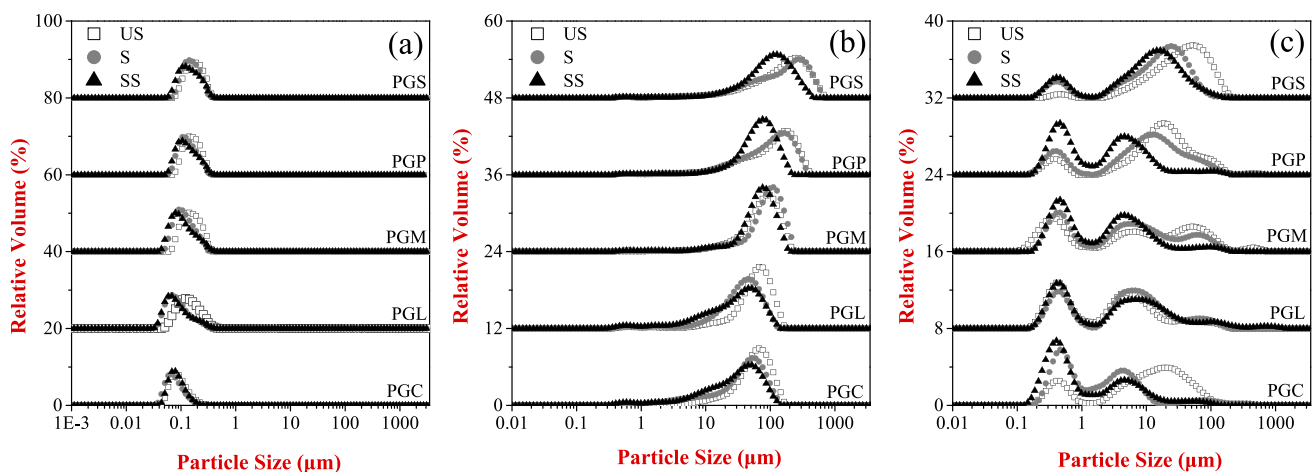


**Fig. 2** Particle size distributions in the nanoemulsions stabilized by PGFEs at different concentrations. **a** initial phase; **b** stomach phase; **c** intestinal phase. Relative volume (%) was stacked up the y-axis for

comparison. US=at the unsaturated concentration; S=at the saturated concentration; SS=at the supersaturated concentration

surfaces, while shorter ones caused smaller particle sizes in the emulsions at their saturated concentration due to their rapid adsorption dynamics based on their small size and low molecular weight [24, 25]. However, Peng et al. [17] showed that emulsions stabilized by long-chain PGFEs (L-PGFEs) had shown the smallest particle sizes compared with those of medium and short ones. The contradictory results obtained may be related to low PGFEs concentrations (<1.0%, w/w) used in previous study at which L-PGFEs emulsions remained stable containing small particle sizes, but other PGFEs emulsions were still unstable with coalesced droplets.

After exposure to the stomach phase, particle sizes of all PGFE-NEs drastically increased up to 40~200  $\mu\text{m}$  (Figs. 1b and 2b). In agreement with our findings, Wang et al. [14] reported emulsions stabilized by PGFEs with low glycerol polymerization degree ( $n=3$ ) were less stable during the stomach digestion with a marked increase in the particle sizes. A remarkable destabilization induced by PGFEs may be attributed to the small polyglycerol head group unable to produce strong steric hindrance to resist against lower pH occurring in the gastric conditions [14]. Nonetheless, a relative reduction in the particle sizes was seen when increasing PGFEs concentrations or decreasing the aliphatic chain lengths of PGFEs (Fig. 1b). One possible explanation was that shorter aliphatic chain or greater concentrations of PGFEs, which were in the aqueous phase, could rapidly adsorb onto the droplet surfaces during agitation, contributing to the redispersion of aggregated droplets within the GIT [24].

At the end of the small intestinal digestion, particle sizes of all the chyme remarkably decreased down to 6~44  $\mu\text{m}$  (Fig. 1c), but were still larger than those of the initial PGFE-NEs (Fig. 1a). The reduction in the particle sizes may be

explained by the following physicochemical processes occurring the intestinal phase including: (i) the redispersion of aggregated droplets; (ii) the hydrolysis of lipid droplets; (iii) and the formation of various colloid particles (e.g. micelles and vesicles) [7]. Interestingly, there were multimodal particle size distributions in the digesta, consisting of an intensity peak of small particles around 0.5  $\mu\text{m}$  in diameter and one or more intensity peaks of large particles ranging between 5 and 80  $\mu\text{m}$  in diameter (Fig. 2c). The former suggested the presence of micelles and vesicles which could accommodate lipolysis products and lipophilic nutraceuticals, whereas the latter indicated the appearance of undigested droplets and insoluble calcium soaps [7]. Moreover, the area of the intensity peak of small particles was larger, while the intensity peaks of large particles were downwards when increasing PGFEs concentrations (Fig. 2c). One possible explanation was that FFAs released from PGFEs hydrolysis may participate in the formation of micelles, resulting in higher levels of micelles [23]. On the other hand, an opposite change in the particle size distributions occurred with an increase in the aliphatic chain lengths of PGFEs, which may be ascribed to the fact that FFAs generated from longer aliphatic chain of PGFEs were prone to form insoluble calcium soaps induced by calcium ions [26].

### $\zeta$ -Potential

All the initial PGFE-NEs contained negative charges ranging between  $-17.4$  and  $-34.1$  (Fig. 3a). Similar to our observations, emulsions stabilized by nonionic surfactants have evidenced to exhibit negative charges probably due to the present of anionic impurities (e.g. FFAs) in the surfactants or lipid phase, and the preferential adsorption of hydroxyl ions from the aqueous phase [24].

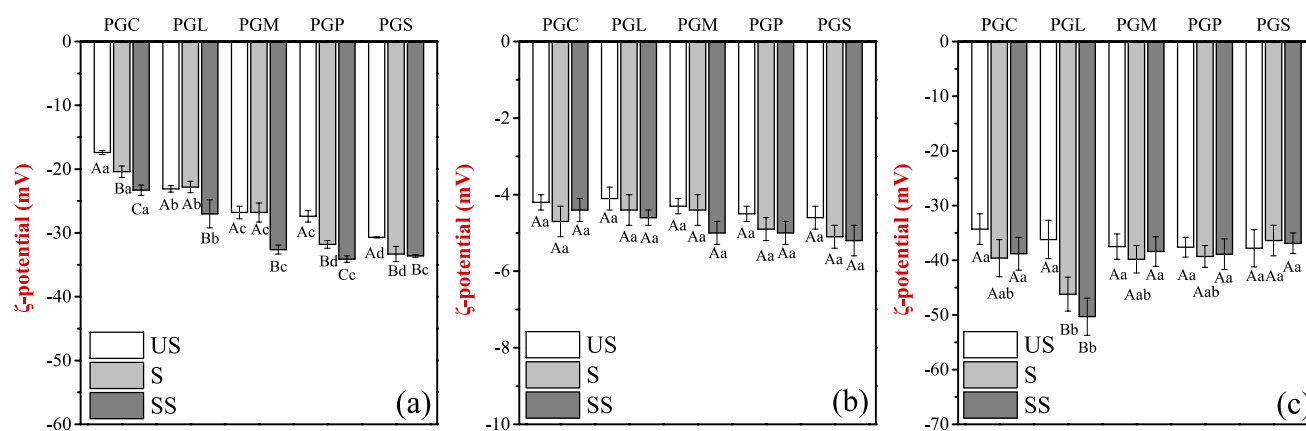


**Fig. 3**  $\zeta$ -potential in the nanoemulsions stabilized by PGFEs at different concentrations. **a** initial phase; **b** stomach phase; **c** intestinal phase. Different capital letters indicate significant differences ( $p < 0.05$ ) among nanoemulsions stabilized by the same PGFEs at different concentrations. Different lowercase letters indicate significant

differences among nanoemulsions stabilized by different PGFEs at concentrations of the same saturation degree (the same gray scale in bars). US = at the unsaturated concentration; S = at the saturated concentration; SS = at the supersaturated concentration

$\zeta$ -potential of all PGFE-NEs drastically increased up to values between  $-5.4$  and  $-3.9$  mV after gastric digestion (Fig. 3b), which may be explained by the reduction in the electrostatic repulsion among the droplets caused by low pH and high ionic strength in the gastric conditions [27].

During the intestinal digestion, more negative charges on the droplets were observed in all the digesta, with values ranging between  $-34.3$  and  $-50.3$  mV (Fig. 3c). There were several physicochemical events responsible for more negative charges on the droplets at the end of the intestinal digestion, including the increase in pH in the digesta, the accumulation of lipolysis products at the interfaces, as well as the adsorption of bile salts and lipase onto the droplet surfaces [28].

### Curcumin Level

Encapsulation efficiency of curcumin in initial PGFE-NEs were almost 95%, with no significant difference ( $p > 0.05$ ) among samples (Fig. 4a), indicating PGFEs can effectively encapsulate curcumin without being affected by the aliphatic chain lengths or concentrations of PGFEs. However, curcumin level of nanoemulsions drastically decreased during the GIT digestion with curcumin retention rate in PGFE-NEs after the small intestinal digestion being between 25.4% and 31.6%, and there was a slight increase in curcumin retention rate of PGFE-NEs (except for PGM-NE) when increasing PGFEs concentrations (Fig. 4b). Chemical stability of lipophilic nutraceuticals in nanoemulsions has reported to be highly associated with the stability of nanoemulsions, because stable droplets contained the intact interfacial layer which can protect nutraceuticals from chemical degradation induced by external environment (such as heat, light

and pH) [29, 30]. Hence, a sharp reduction in curcumin of PGFE-NEs along the GIT was presumably ascribed to the destabilization of nanoemulsions occurring in the stomach digestion, and an increase in PGFEs concentration may be beneficial to the stability of nanoemulsions, thereby to some extent improving curcumin stability.

### Lipolysis Dynamics during the Intestinal Digestion

Lipolysis profiles of PGFE-NEs were monitored through released FFA (%) during the intestinal digestion. In order to deeply understand lipolysis dynamics of PGFE-NEs, the time to approach effective lipolysis ( $T_c$ ) and the rate constant ( $k$ ) obtained from the three-parameter logistics model were used to indicate the initial lag time and the rate of lipid digestion, relatively.

In general, PGFE-NEs presented a rapid FFAs release at the early 30 min, followed by a gradual increase until the plateau was reached, with the exception of PGC-NE at a high concentration and PGP-NE at a low concentration where an initial lag time occurred (Fig. 5), which were consistent with longer  $T_c$  values (Fig. 6a). An initial lag time observed indicated that lipase was unable to rapidly adsorb onto the interfaces and hydrolyze oil droplets, possibly because of less surface area exposed to lipase or barrier protection from emulsifiers [19].

PGFEs concentrations had little impact on lipid digestion of PGL-NE, PGM-NE and PGS-NE, showing no significant change in  $T_c$  values,  $k$  values and FFAs (%) when increasing PGFEs concentrations (Fig. 6). However, PGC-NE displayed not only slower lipolysis dynamics with a longer  $T_c$  value (from  $16.7 \pm 0.3$  to  $28.3 \pm 0.7$  min) and lower  $k$  value (from  $0.146 \pm 0.005$  to  $0.093 \pm 0.005$   $\text{min}^{-1}$ ), but also a

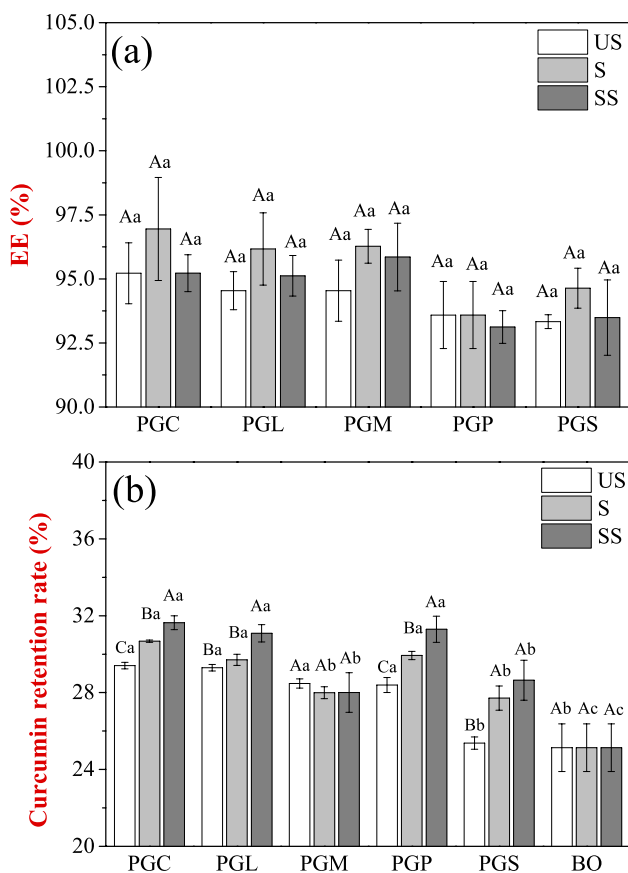


**Fig. 4** Encapsulation efficiency (a) of curcumin in the initial nanoemulsions and retention rate (b) of curcumin in nanoemulsions after the intestinal digestion. Different capital letters indicate significant differences ( $p < 0.05$ ) among nanoemulsions stabilized by the same PGFEs at different concentrations. Different lowercase letters indicate significant differences among nanoemulsions stabilized by different PGFEs at concentrations of the same saturation degree (the same gray scale in bars). US = at the unsaturated concentration; S = at the saturated concentration; SS = at the supersaturated concentration

lower extent of lipolysis (from  $74.1 \pm 0.6$  to  $48.2 \pm 1.7\%$ ) as PGC concentration increasing (Fig. 6). A sufficiently high concentration of low-mass surfactant has been demonstrated to form a dense adsorption layer at the interfaces which makes it difficult for the displacement and adsorption of lipase and bile salts, thus resulting in the suppression on lipid hydrolysis [31]. Therefore, the inhibitory effect of PGC on lipid digestion may be due to a higher concentration of PGC (4–8%) used in the present study. Conversely, PGP-NE presented different behaviors of lipid digestion that oil droplets were more rapidly hydrolyzed with  $T_c$  value decreasing from  $65.2 \pm 0.7$  to  $11.3 \pm 0.3$  min and  $k$  value increasing from  $0.095 \pm 0.006$  to  $0.189 \pm 0.009 \text{ min}^{-1}$ , while there was no significant difference in lipolysis degree when a greater level of PGP was applied (Fig. 6). In fact, lipolysis dynamics is greatly determined by the aggregation state of the droplets exposed to the intestinal phase, and more aggregated

droplets may lead to a slower rate of lipid digestion having less effect on the extent of lipolysis [32]. Consequently, it can imply that, PGP-NE at a low concentration underwent extensive coalescence during the intestinal digestion, and an increase in PGP concentration may contribute to the redispersion of coalesced droplets, which facilitated the accessibility of lipase to the droplet surfaces and the rate of lipid hydrolysis [7].

On the other hand, the aliphatic chain lengths of PGFEs played a crucial role in both lipolysis dynamics and lipolysis degree. The data of PGC-NE and PGP-NE used for the analysis on the effect of the aliphatic chain lengths in PGFEs on lipid digestion was chosen as that of PGC-NE at the unsaturated concentration and PGP-NE at the supersaturated concentration, respectively, to avoid the influence of PGFEs concentrations. Longer aliphatic chain of PGFEs induced a more rapid lipid hydrolysis presenting a lower  $T_c$  value and a greater  $k$  value. Furthermore, a greater extent of lipolysis was observed when increasing the aliphatic chain lengths of PGFEs. Medium-chain FFAs released from lipolysis are prone to migrate into the aqueous phase, without affecting lipid digestion. On the contrary, long-chain FFAs released tend to accumulate at the interfaces, which retards continuous hydrolysis of lipase on oil droplets. However, in the case of sufficient calcium ions in the digestive fluids, long-chain FFAs surrounding the droplets would be removed and precipitated by calcium ions, thereby promoting lipid hydrolysis [33, 34]. As a consequence, the difference in water dispersibility of FFAs released from PGFEs may be responsible for an enhanced lipolysis induced by longer aliphatic chain of PGFEs.

### Curcumin Bioaccessibility

Curcumin bioaccessibility of PGFE-NEs was determined at the end of the intestinal digestion. Irrespective of the concentrations used, medium-chain PGFE-NEs presented a greater curcumin bioaccessibility than long-chain ones (Fig. 7). Moreover, the former showed a slight increase in curcumin bioaccessibility as PGFEs concentrations increasing, while the latter exhibited a significant reduction ( $p < 0.05$ ) in curcumin bioaccessibility (Fig. 7). The inverse changes observed suggested that there were different mechanisms of action in PGFEs on curcumin bioaccessibility depending on their aliphatic chain.

In fact, nutraceutical bioaccessibility has been widely reported to have a positive relationship with the extent of lipid hydrolysis, presumably because a higher extent of lipolysis may contribute to a higher level of the micelles which could enhance the micellization of nutraceuticals [35]. However, our study got different results that there was a greater extent of lipolysis but a lower amount of curcumin bioaccessibility in the nanoemulsions stabilized by longer

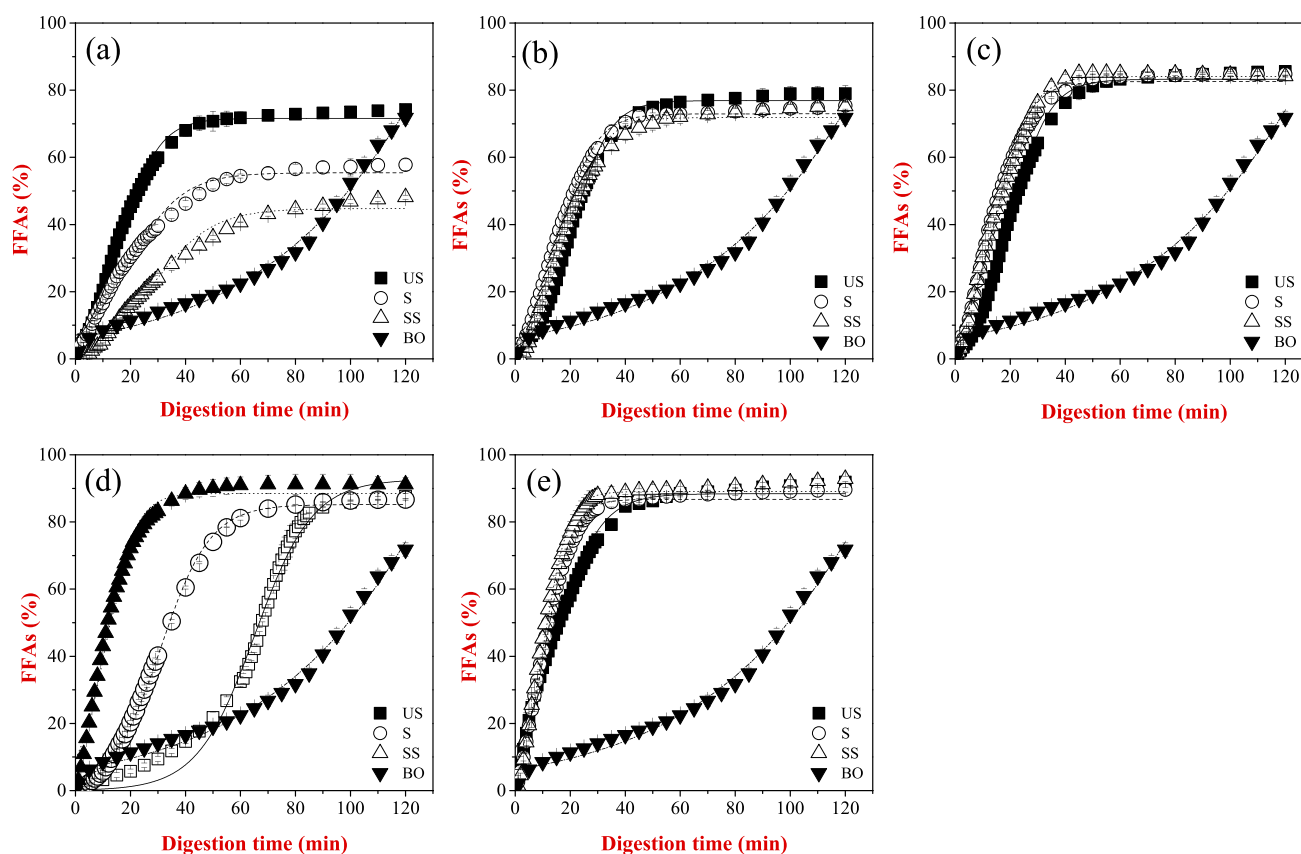


**Fig. 5** FFAs (%) released during the intestinal digestion of nanoemulsions stabilized by PGFEs. **a** PGC-NE; **b** PGL-NE; **c** PGM-NE; **d** PGP-NE; **e** PGS-NE. The symbols represent the experimental data, while corresponding lines indicate the predicted values from the

three-parameter logistic model. **US**=at the unsaturated concentration; **S**=at the saturated concentration; **SS**=at the supersaturated concentration; **BO**=bulk oil

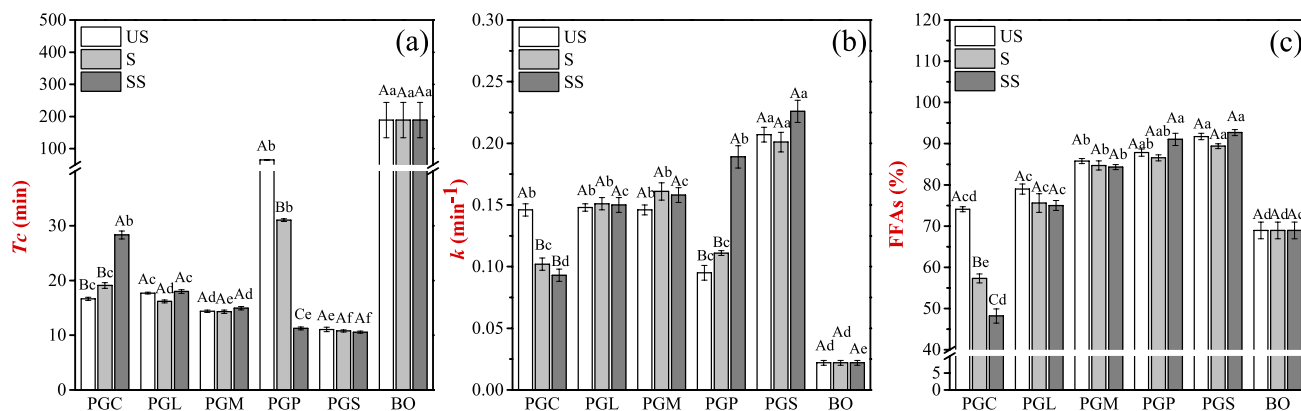


**Fig. 6** Estimated parameters obtained from the three-parameter logistics model. **a** the time to achieve effective lipolysis ( $T_c$ ); **b** rate constant ( $k$ ); **c** released FFAs (%). Different letters indicate significant

differences ( $p < 0.05$ ) among nanoemulsions. **US**=at the unsaturated concentration; **S**=at the saturated concentration; **SS**=at the supersaturated concentration; **BO**=bulk oil

aliphatic chain of PGFEs (Fig. 7), implying there were other factors having more direct impact on curcumin bioaccessibility than lipolysis degree. Previous studies reported that higher levels of calcium ions resulted in a greater extent

of lipolysis but a lower bioaccessibility of lipophilic nutraceuticals (e.g. curcumin,  $\beta$ -carotene, vitamin E and carotenoids), which was attributed to the precipitation of FFAs required for form micelles [26, 34, 36, 37]. Therefore, the

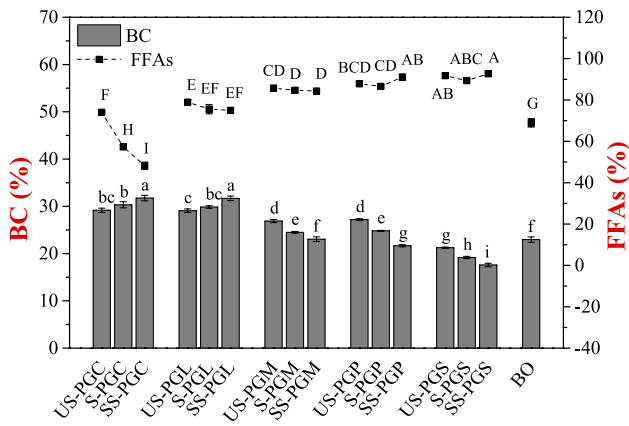


**Fig. 7** Curcumin bioaccessibility (BC%) (bars) and FFAs (%) (lines) released from nanoemulsions. Different capital letters indicate significant differences ( $p < 0.05$ ) in FFAs (%), while different lowercase letters indicate significant differences in BC%. **US-PGFEs** = PGFEs-NE at the unsaturated concentration; **S-PGFEs** = PGFEs-NE at the saturated concentration; **SS-PGFEs** = PGFEs-NE at the supersaturated concentration; **BO** = bulk oil

distributions of curcumin during micellization process might be the main factor determining curcumin bioaccessibility [38, 39]. For this reason, the ratio of curcumin concentrations in the micelles versus in the digesta, referred as micellar transfer rate (MT%), was determined to evaluate the distributions of curcumin between the micelle phase and the sediment phase at the end of digestion.

MT% positively correlated with curcumin bioaccessibility in all tested digesta (Fig. 8). For medium-chain PGFE-NEs, curcumin released was almost completely incorporated into the micelles with MT% being approximately

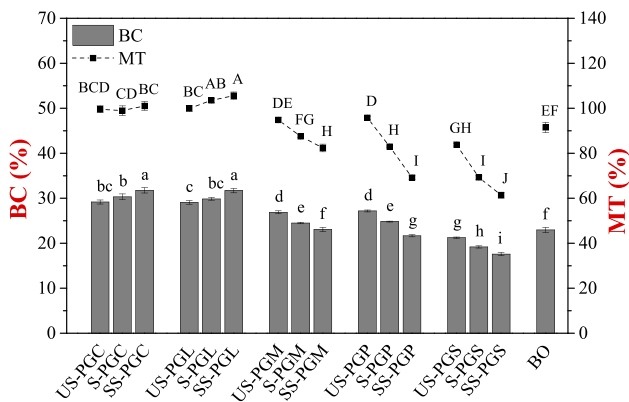


**Fig. 8** Curcumin bioaccessibility (BC%) (bars) and micellar transfer rate (MT%) (lines) at the end of the intestinal digestion. Different capital letters indicate significant differences ( $p < 0.05$ ) in MT%, while different lower case letters indicate significant differences in BC%. **US-PGFEs** = PGFEs-NE at the unsaturated concentration; **S-PGFEs** = PGFEs-NE at the saturated concentration; **SS-PGFEs** = PGFEs-NE at the supersaturated concentration; **BO** = bulk oil

100%, and a slight increase in MT% was observed when a higher level of PGFEs were used. However, MT% of long-chain PGFE-NEs was significantly lower ( $p < 0.05$ ) than that of medium-chain ones, and MT% significantly decreased ( $p < 0.05$ ) with an increase in the aliphatic chain lengths or concentrations of PGFEs (Fig. 8). These results were supported by visual observations of the digesta after centrifugation where there was a greater amount of the precipitation produced along with more curcumin caught in the precipitation at the bottom of the tubes in long-chain PGFE-NEs than medium-chain PGFE-NEs (Fig. 9). Medium aliphatic chain of PGFEs could facilitate the micellization of curcumin probably because corresponding FFAs released were prone to migrate into the micelles and further improve solubilization capacity of the micelles. On the contrary, FFAs generated from long aliphatic chain of PGFEs would tend to bind with calcium ions and form insoluble calcium soaps, which resulted in more curcumin trapped within the sediment phase and therefore lowered curcumin bioaccessibility [34, 40]. Our results are in accordance with Fan et al. [41] reporting how the aliphatic chain lengths of Tween ( $C_{12:0}$ ,  $C_{16:0}$ ,  $C_{18:0}$ ,  $C_{18:1}$ ) affect  $\beta$ -carotene (BC) bioaccessibility in organogel-based

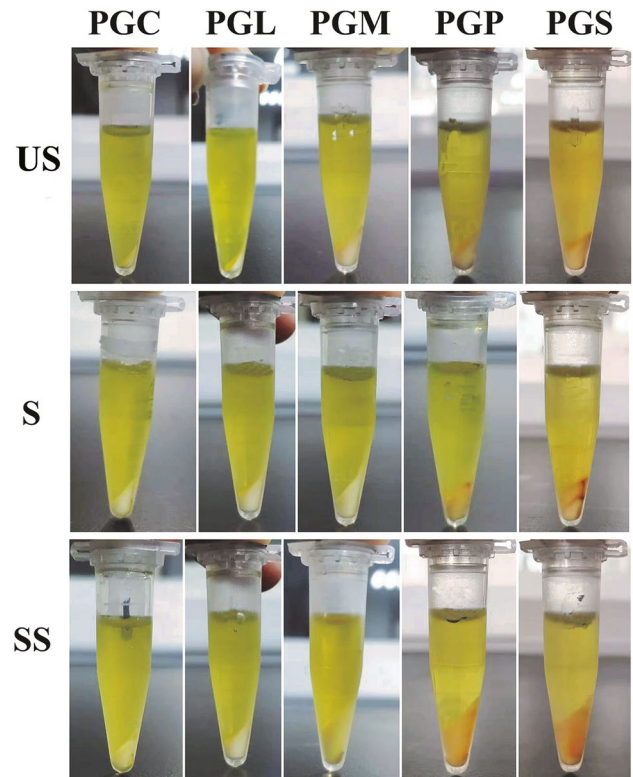


**Fig. 9** Visual appearance of centrifugation separation in the digesta after the intestinal digestion (note the level and color of the sediments at the bottom of the tubes). **US** = at the unsaturated concentration; **S** = at the saturated concentration; **SS** = at the supersaturated concentration

nanoemulsions and nanoemulsion stabilized by Tween 20 (C<sub>12</sub>) presenting the greatest BC bioaccessibility. Consequently, lipid-based surfactants with medium aliphatic chain may be more suitable for encapsulating and delivering nutraceuticals compared with those with long aliphatic chain.

## Conclusions

The aliphatic chain lengths or the concentrations of PGFEs had a pivotal impact on the physicochemical stability, lipolysis dynamics and curcumin bioaccessibility in curcumin-enriched nanoemulsions. Even though all PGFEs induced emulsion destabilization under gastric conditions, there were relatively smaller particle sizes along the GIT when shorter aliphatic chain or greater concentrations of PGFEs were applied. PGFEs concentrations had little impact on lipid digestion of nanoemulsions except for those stabilized by PGC and PGP. Moreover, long-chain PGFE-NEs presented a greater rate and extent of lipid digestion, but a lower amount of curcumin bioaccessibility than medium-chain ones, indicating curcumin bioaccessibility was more dependent on FFAs species than the total amount of FFAs. This work highlights the importance of the aliphatic chain lengths in PGFEs for the rational design of emulsion-based systems to encapsulate lipophilic nutraceuticals.

**Supplementary Information** The online version contains supplementary material available at <https://doi.org/10.1007/s11483-021-09681-z>.

**Acknowledgements** This work was funded by the Key Research and Development Program of Guangdong Province (No. 2019B020213001). We thank Dr. Song Zhang and Dr. Linshang Zhang for their constructive advices in the design of experiment.

**Funding** This work was funded by the Key Research and Development Program of Guangdong Province (No. 2019B020213001).

**Data Availability** The data and material that support the findings of this study are available from the corresponding author upon reasonable request.

**Code Availability** Not applicable.

## Declarations

**Ethics Approval** Not applicable.

**Consent to Participate** Not applicable.

**Consent for Publication** Not applicable.

**Conflict of Interest** There is no conflict to declare.

## References

1. B. Han, B.X. Hoang, J. Infect. Publ. Health **13**, 1811–1817 (2020)
2. V. Raikos, V. Ranawana, Int. J. Food Sci. Technol. **52**, 68–80 (2017)
3. S.J. Choi, D.J. McClements, Food Sci. Biotechnol. **29**, 149–168 (2020)
4. Q.Q. Liu, H. Huang, H.H. Chen, J.F. Lin, Q. Wang, Molecules **24**, 4242 (2019)
5. L. Salvia-Trujillo, C. Qian, O. Martin-Belloso, D.J. McClements, Food Chem. **141**, 1472–1480 (2013)
6. D.J. McClements, Food Funct. **9**, 22–41 (2018)
7. S.H.E. Verkempinck, L. Salvia-Trujillo, L.G. Moens, et al., Food Chem. **246**, 179–191 (2018)
8. Y. Li, D.J. McClements, Eur. J. Pharm. Biopharm. **79**, 423–431 (2011)
9. J. Feng, M.G. Huang, Z. Chai, et al., Food Funct. **11**, 5223–5239 (2020)
10. C. Qian, E.A. Decker, H. Xiao, D.J. McClements, Food Chem. **135**, 1440–1447 (2012)
11. K.S. Shikhaliev, N.V. Stolpovskaya, M.Y. Krysin, et al., J. Am. Oil Chem. Soc. **93**, 1429–1440 (2016)
12. S. Zhang, J. Xiong, W.Y. Lou, Z.X. Ning, D.H. Zhang, J.G. Yang, Food Control **98**, 113–119 (2019)
13. L.-J. Yin, I. Kobayashi, M. Nakajima, Food Biophysics. **3**, 213–218 (2008)
14. Z. Wang, M.A. Neves, L.-J. Yin, I. Kobayashi, K. Uemura, M. Nakajima, Food Sci. Technol. Res. **18**, 149–156 (2012)
15. B. Kocaadam, N. Sanlier, Crit. Rev. Food Sci. **57**, 2889–2895 (2017)
16. A.B. Kunnumakkara, D. Bordoloi, G. Padmavathi, et al., Br. J. Pharmacol. **174**, 1325–1348 (2017)
17. B. Peng, C.Y. Xiong, Y. Huang, J.N. Hu, X.M. Zhu, Z.Y. Deng, J. Agric. Food Chem. **66**, 8104–8113 (2018)
18. B.J. Zheng, S.F. Peng, X.Y. Zhang, D.J. McClements, J. Agric. Food Chem. **66**, 10816–10826 (2018)
19. N. Ng, P.X. Chen, S.M. Ghazani, et al., Food Funct. **10**, 8195–8207 (2019)
20. J. Xiao, C. Lo, Q.R. Huang, J. Agric. Food Chem. **63**, 10263–10270 (2015)
21. K.F. Yao, D.J. McClements, J.X. Xiang, et al., Food Funct. **10**, 5302–5311 (2019)
22. L. Zou, B. Zheng, W. Liu, C. Liu, H. Xiao, D.J. McClements, J. Funct. Foods **15**, 72–83 (2015)
23. H. Helena de Abreu-Martins, M. Artiga-Artigas, R. Hilsdorf Piccoli, O. Martin-Belloso, L. Salvia-Trujillo, Food Chem. **311**, 126024 (2020)
24. A. Gasa-Falcon, I. Odriozola-Serrano, G. Oms-Oliu, O. Martin-Belloso, Food Funct. **10**, 713–722 (2019)
25. C. Qian, D.J. McClements, Food Hydrocoll. **25**, 1000–1008 (2011)
26. Q. Lin, R. Liang, A. Ye, H. Singh, F. Zhong, Food Hydrocoll. **73**, 184–193 (2017)
27. R.J. Zhang, Z.P. Zhang, H. Zhang, E.A. Decker, D.J. McClements, Food Hydrocoll. **45**, 175–185 (2015)
28. B. Ozturk, S. Argin, M. Ozilgen, D.J. McClements, Food Chem. **187**, 499–506 (2015)
29. C.P. Tan, M. Nakajima, J. Sci. Food Agric. **85**, 121–126 (2005)
30. H. Jin, C. Liu, S.Y. Zhang, et al., Food Funct. **11**, 10205–10218 (2020)
31. Z. Vinarov, Y. Petkova, S. Tcholakova, et al., Langmuir **28**, 8127–8139 (2012)
32. M. Golding, T.J. Wooster, L. Day, et al., Soft Matter **7**, 3513–3523 (2011)

33. R.J. Zhang, Z.P. Zhang, H. Zhang, E.A. Decker, D.J. McClements, *Food Res. Int.* **75**, 71–78 (2015)
34. Y. Yang, E.A. Decker, H. Xiao, D.J. McClements, *Food Funct.* **6**, 84–97 (2015)
35. Y.B. Tan, Z.Y. Zhang, J.N. Liu, H. Xiao, D.J. McClements, *Food Funct.* **12**, 2338–2338 (2021)
36. Y.Q. Pei, T.Y. Ai, Z.Y. Deng, et al., *Food Funct.* **10**, 3344–3355 (2019)
37. J. Corte-Real, M. Iddir, C. Soukoulis, E. Richling, L. Hoffmann, T. Bohn, *Food Chem.* **197**, 546–553 (2016)
38. Y.B. Tan, R.Y. Li, C.Z. Liu, et al., *Food Funct.* **11**, 187–199 (2020)
39. Y. Tan, Z. Zhang, J.M. Mundo, D.J. McClements, *Food Res. Int.* **137**, 109739 (2020)
40. M. Hu, Y. Li, E.A. Decker, D.J. McClements, *Food Hydrocoll.* **24**, 719–725 (2010)
41. Y.T. Fan, L.Y. Gao, J. Yi, Y.Z. Zhang, W. Yokoyama, *J. Agric. Food Chem.* **65**, 6188–6194 (2017)

**Publisher's Note** Springer Nature remains neutral with regard to jurisdictional claims in published maps and institutional affiliations.